


# Surface phonon resonance: A new mechanism for enhancing photonic spin Hall effect and refractive index sensor

Jie Cheng(程杰), Chenglong Wang(汪承龙), Yiming Li(李一铭), Yalin Zhang(张亚林), Shengli Liu(刘胜利), and Peng Dong(董鹏)

**Citation:**Chin. Phys. B, 2024, 33 (**8**): 084201. DOI: 10.1088/1674-1056/ad4a3c

**What follows is a list of articles you may be interested in**

---

## Multi-functional photonic spin Hall effect sensor controlled by phase transition

Jie Cheng(程杰), Rui-Zhao Li(李瑞昭), Cheng Cheng(程骋), Ya-Lin Zhang(张亚林), Sheng-Li Liu(刘胜利), and Peng Dong(董鹏)

Chin. Phys. B, 2024, 33 (**7**): 074203. DOI: 10.1088/1674-1056/ad3b85

## Engineered photonic spin Hall effect of Gaussian beam in antisymmetric parity-time metamaterials

Lu-Yao Liu(刘露遥), Zhen-Xiao Feng(冯振校), Dong-Mei Deng(邓冬梅), and Guang-Hui Wang(王光辉)

Chin. Phys. B, 2023, 32 (**9**): 094201. DOI: 10.1088/1674-1056/accb89

## Asymmetrical photonic spin Hall effect based on dielectric metasurfaces

Guangzhou Geng(耿广州), Ruhao Pan(潘如豪), Wei Zhu(朱维), and Junjie Li(李俊杰)

Chin. Phys. B, 2022, 31 (**12**): 124207. DOI: 10.1088/1674-1056/ac754b

## Enhancing terahertz photonic spin Hall effect via optical Tamm state and the sensing application

Jie Cheng(程杰), Jiahao Xu(徐家豪), Yinjie Xiang(项寅杰), Shengli Liu(刘胜利), Fengfeng Chi(迟逢逢), Bin Li(李斌), and Peng Dong(董鹏)

Chin. Phys. B, 2022, 31 (**12**): 124202. DOI: 10.1088/1674-1056/ac92d5

## Photonic spin Hall effect and terahertz gas sensor via InSb-supported long-range surface plasmon resonance

Jie Cheng(程杰), Gaojun Wang(王高俊), Peng Dong(董鹏), Dapeng Liu(刘大鹏), Fengfeng Chi(迟逢逢), and Shengli Liu(刘胜利)

Chin. Phys. B, 2022, 31 (**1**): 014205. DOI: 10.1088/1674-1056/ac192a

---

# Surface phonon resonance: A new mechanism for enhancing photonic spin Hall effect and refractive index sensor

Jie Cheng(程杰)[1,†], Chenglong Wang(汪承龙)[2], Yiming Li(李一铭)[1], Yalin Zhang(张亚林)[1], Shengli Liu(刘胜利)[1], and Peng Dong(董鹏)[3,‡]

[1] *School of Science, Jiangsu Province Engineering Research Center of Low Dimensional Physics and New Energy, Nanjing University of Posts and Telecommunications, Nanjing* 210023, *China*

[2] *College of Electronic and Optical Engineering, Nanjing University of Posts and Telecommunications, Nanjing* 210023, *China*

[3] *School of Electrical Engineering, Research Center of Intelligent Sensor and Network Engineering Technology of Jiangsu Province, Nanjing Vocational University of Industry Technology, Nanjing* 210023, *China*

(Received 3 April 2024; revised manuscript received 9 May 2024; accepted manuscript online 13 May 2024)

Metal-based surface plasmon resonance (SPR) plays an important role in enhancing the photonic spin Hall effect (SHE) and developing sensitive optical sensors. However, the very large negative permittivities of metals limit their applications beyond the near-infrared regime. In this work, we theoretically present a new mechanism to enhance the photonic SHE by taking advantage of SiC-supported surface phonon resonance (SPhR) in the mid-infrared regime. The transverse displacement of photonic SHE is very sensitive to the wavelength of incident light and the thickness of SiC layer. Under the optimal parameter setup, the calculated largest transverse displacement of SiC-based SPhR structure reaches up to 163.8 μm, which is much larger than the condition of SPR. Moreover, an $NO_2$ gas sensor based on the SPhR-enhanced photonic SHE is theoretically proposed with the superior sensing performance. Both the intensity and angle sensitivity of this sensor can be effectively manipulated by varying the damping rate of SiC. The results may provide a promising paradigm to enhance the photonic SHE in the mid-infrared region and open up new opportunity of highly sensitive refractive index sensors.

**Keywords:** photonic spin Hall effect, refractive index sensor, surface phonon resonance, SiC

**PACS:** 42.25.–p, 41.20.Jb, 42.79.–e, 78.20.Ci **DOI:** 10.1088/1674-1056/ad4a3c

## 1. Introduction

Surface polaritons, as the surface electromagnetic waves propagating along a surface of a medium, have aroused significant attention both experimentally and theoretically due to their revolutionary sensing applications in environmental monitoring, food safety, and medical diagnostics.[1–3] Generally, polaritons can be classified into three different types: plasmon polariton, exciton polariton, and phonon polariton. Among them, surface plasmon polariton is the mostly well-studied one, and metals-based plasmon has led to much advancement such as improved chemical detection from the ultraviolet to near-infrared spectral ranges.[4–6] However, their very large negative permittivity at longer wavelengths limits their utilizations beyond the near-infrared regime.[7] Surface phonon polariton, which originates from the interaction between the electromagnetic fields and phonons (lattice vibrations) of polar dielectric materials (SiC, $SiO_2$, BN, *etc.*), can be considered as a mid-infrared counterpart of surface plasmon polariton.[8–10] Similar to surface plasmon resonance (SPR), surface phonon resonance (SPhR) exhibits a narrow resonance spectrum with Lorentz shape. In recent years, optical sensors based on SPhR operating in the mid-infrared range have been successively proposed and demonstrated with superior sensing performance.[11–13] Note that, the polar dielectric materials usually have more durability than metals, which make them attractive in sensing applications for chemically aggressive analytes.

As a novel optical phenomenon, photonic spin Hall effect (SHE) provides a new platform for precision metrology and sensitive sensing.[14–16] The photonic SHE is an optical analogy of SHE in electronic systems, where the spin photons and refractive index gradient play the roles of spin electrons and electric potential gradient, respectively. The photonic SHE manifests itself as the spin-dependent transverse splitting of left- and right-handed circularly polarized components when a light beam reflects or refracts at an inhomogeneity interface, originating from the spin–orbit interaction between the photon spin (polarization) and the light beam trajectory (orbit angular momentum).[17–19] Due to the high sensitivity of transverse displacements on physical parameters in material, the photonic SHE exhibits the unique potential for applications in precision metrology, such as the measurement of metal film thickness,[20] the identification of graphene layer numbers[21] and ultrasensitive detection of ion concentration in solution.[22] Furthermore, any changes in the refractive index of sensing medium will result in the great variation of spin

†Corresponding author. E-mail: chengj@njupt.edu.cn
‡Corresponding author. E-mail: 2021101298@niit.edu.cn

© 2024 Chinese Physical Society and IOP Publishing Ltd 

displacements in photonic SHE.[23–25] Therefore, the photonic spin-Hall displacements offer important information of the optical interface, making it to be exploited as the effective pointer for surface analysis and refractive index sensing. In addition, it is important to note that, in contrast to conventional sensors based on surface polaritons, the photonic SHE sensors exhibit the excellent sensitivity, desirable accuracy and high signal-to-noise ratio.[26] Until now, the photonic SHE sensing scheme have been theoretically put forward in the real-time analysis of gas environment[27] and highly sensitive detection of DNA hybridization,[28] by taking advantage of surface polariton- (*e.g.* SPR or surface exciton polariton) enhanced spin displacements.[29–32] However, as another type of surface polaritons, there are few reports on the relationship between SPhR and photonic SHE. Questions naturally arise: whether it is possible to enhance the photonic SHE by SPhR? If yes, can we design a novel refractive index sensor based on the SPhR-enhanced photonic SHE?

In this work, we proposed a new mechanism for enhancing photonic SHE and refractive index sensor via SiC-supported SPhR in the mid-infrared regime. Under the optimal parameter setup, the maximal transverse shift of 163.8 μm can be achieved at the incident wavelength of 10.4 μm, which is about 54 times that of SPR condition. A highly sensitive $NO_2$ gas sensing is further investigated, based on the SPhR-enhanced photonic SHE. In addition, the photonic SHE and sensing performance can be effectively tuned by adjusting the damping rate of SiC. Our research provides a promising way to improve and modulate the photonic SHE in the mid-infrared region and may open a platform for developing highly sensitive mid-infrared photonic SHE sensors to detect harmful gases.

## 2. Theory and model

Following the generation of traditional SPR, SPhR can be excited by a typical Kretschmann–Raether configuration,[5] where the metal film is replaced by a surface-phonon-supporting SiC film, as illustrated in Fig. 1(a). The proposed structure comprises a thin layer of SiC deposited over a Ge prism, and the sensing analyte is in contact with the SiC layer. Figure 1(b) shows the atomic lattice oscillations in a polar crystalline material (SiC), with the positively charged and negatively charged lattice points moving in the same and opposite directions of the incident electromagnetic field, resulting in a negative dielectric constant. Analogous to metals, the frequency dependent complex permittivity of SiC can be expressed by the Drude–Lorentz model[9]

$$\varepsilon_{\mathrm{SiC}}(\omega)=\varepsilon'_{\mathrm{SiC}}+\mathrm{i}\varepsilon''_{\mathrm{SiC}}=\varepsilon_{\infty}\frac{\omega^2-\omega_{\mathrm{LO}}^2+\mathrm{i}\gamma\omega}{\omega^2-\omega_{\mathrm{TO}}^2+\mathrm{i}\gamma\omega}, \tag{1}$$

where the longitudinal optical phonon frequency is $\omega_{\mathrm{LO}}=972\ \mathrm{cm}^{-1}$, the transverse optical phonon frequency is $\omega_{\mathrm{TO}}=796\ \mathrm{cm}^{-1}$, the damping rate due to vibrational anharmonicity is set to be $\gamma=3.75\ \mathrm{cm}^{-1}$, and the high-frequency dielectric constant $\varepsilon_{\infty}=6.5$. The reststrahlen band defined by $\varepsilon'_{\mathrm{SiC}}<0$ corresponds to $\omega_{\mathrm{TO}}<\omega<\omega_{\mathrm{LO}}$. The refractive index of Ge prism is given by[33]

$$n_{\mathrm{Ge}}=\sqrt{9.28156+\frac{6.7288\lambda^2}{\lambda^2-0.44105}+\frac{0.21307\lambda^2}{\lambda^2-3870.1}}, \tag{2}$$

in which $\lambda$ is the incident light wavelength in micrometers.

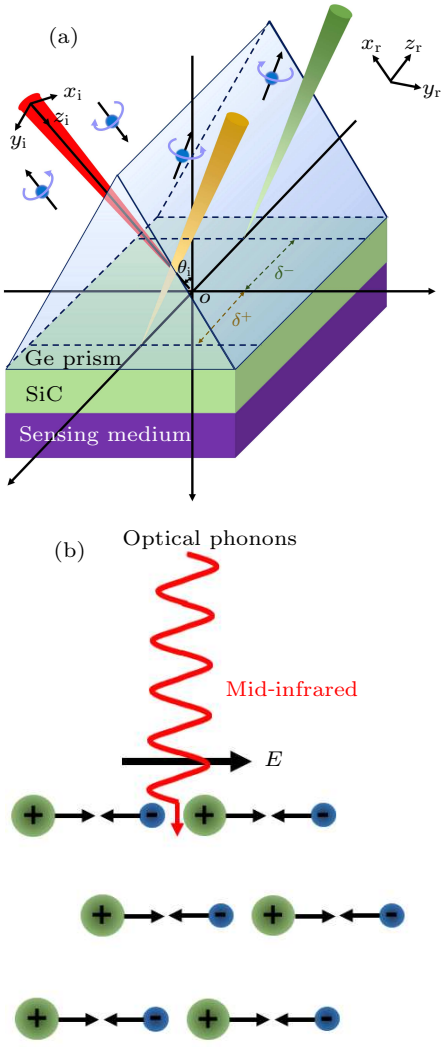



**Fig. 1.** (a) Schematic illustration of photonic SHE in the SPhR structure consisting of Ge prism, SiC, and sensing medium. Here, $\delta^+$ and $\delta^-$ are the transverse displacements of the left- and right-handed circularly polarized components, respectively. (b) Conceptual diagram of atomic displacement in the form of optical phonons for SiC.

A monochromatic Gaussian beam is incident into the SPhR structure of Fig. 1(a) with an incident angle $\theta_i$. Due to the photonic SHE, the reflected light will split into two bundles of left- and right-handed circularly polarized components. In order to calculate the transverse displacements, a general beam propagation model using angular spectrum theory is employed. The angular spectrum of incident beam can be written

as[34]

$$\tilde{E}_{i\pm} = (e_{ix} \pm e_{iy}) \frac{w_0}{\sqrt{2\pi}} \exp\left[ -\frac{(k_{ix}^2 + k_{iy}^2)\omega_0^2}{4} \right], \tag{3}$$

where $w_0$ is the beam waist. By matching the boundary condition, the angular spectrum of the reflected light beam can be expressed as[34]

$$\begin{bmatrix} \tilde{E}_r^H \\ \tilde{E}_r^V \end{bmatrix} = \begin{bmatrix} r_p & \frac{k_{ry}\cot\theta_i (r_p + r_s)}{k_0} \\ \frac{-k_{ry}\cot\theta_i (r_p + r_s)}{k_0} & r_s \end{bmatrix} \begin{bmatrix} \tilde{E}_i^H \\ \tilde{E}_i^V \end{bmatrix}. \tag{4}$$

Here, $\tilde{E}_{r(i)}^H$ and $\tilde{E}_{r(i)}^V$ represent the horizontal (H) and vertical (V) components of the angular spectrum with the reflected and incident beams, respectively. $k_0 = 2\pi/\lambda$ is the wave number in free space. The spin-dependent transverse displacements of reflected light beams can be obtained with[35]

$$\delta_{H,V}^{\pm} = \frac{\iint y_r |\boldsymbol{E}_{H,V}^{\pm}|^2 \mathrm{d}x_r \mathrm{d}y_r}{\iint |\boldsymbol{E}_{H,V}^{\pm}|^2 \mathrm{d}x_r \mathrm{d}y_r}. \tag{5}$$

From Eqs. (3)–(5), it can be obtained that the transverse displacement of the photonic SHE in H and V polarization states is[35]

$$\delta_H^{\pm} = \mp \frac{k_0 w_0^2 \mathrm{Re}(1 + r_s/r_p)\cot\theta_i}{k_0^2 w_0^2 + \left|\frac{\partial \ln r_p}{\partial \theta_i}\right|^2 + \left|(1 + r_s/r_p)\cot\theta_i\right|^2}, \tag{6}$$

$$\delta_V^{\pm} = \mp \frac{k_0 w_0^2 \mathrm{Re}(1 + r_p/r_s)\cot\theta_i}{k_0^2 w_0^2 + \left|\frac{\partial \ln r_s}{\partial \theta_i}\right|^2 + \left|(1 + r_p/r_s)\cot\theta_i\right|^2}. \tag{7}$$

Here $r_{p,s} = |r_{p,s}| \exp(i\varphi_{p,s})$ are the Fresnel reflection coefficients for the H and V polarization states, which can be determined by the transfer matrix method. It is obvious that the transverse displacements for left- and right-circularly polarized light are the same in magnitude but opposite in sign, and the value is intimately related to the ratio between $r_p$ and $r_s$. For simplicity, we only present the case of the left- circularly polarized component in the following discussion.

## 3. Simulation results and analysis

Figure 2(a) shows the real and imaginary part of the SiC permittivity as a function of incident light wavelength. In order to excite phonon polaritons, the real part of the permittivity for the phonon material must be negative, corresponding to the so-called Reststrahlen band.[10] This condition is similar to the negative permittivity of the plasmonic materials below their plasma frequency.[8] For the phononic material SiC in this work, the Reststrahlen band ranges from 10.3 μm to 12.5 μm. It should be noted that, this Reststrahlen band defines the operational range of SPhR devices; and the changes of crystal lattice properties for SiC can effectively modify the Reststrahlen band. Therefore, the applications of SPhR optical devices in a broad or adaptable frequency range are anticipated.[10] To further confirm the excitation of phonon polaritons within this Reststrahlen band, we provide the reflection coefficient $|r_p|$ for Ge prism-SiC-air structure (with a random SiC thickness of $d = 650$ nm) at the wavelength region of 10.3 μm–11.0 μm. As shown in Figs. 2(b) and 2(c), the reflection coefficient produces an obvious resonance dip at each incident wavelength, which is mainly caused by the SPhR effect. In the following calculation, the wavelength of incident light is arbitrarily set to be 10.6 μm with a beam waist of 0.5 mm, and the complex dielectric constant of the SiC is calculated as $\varepsilon_{SiC} = -1.39 + 0.11i$.

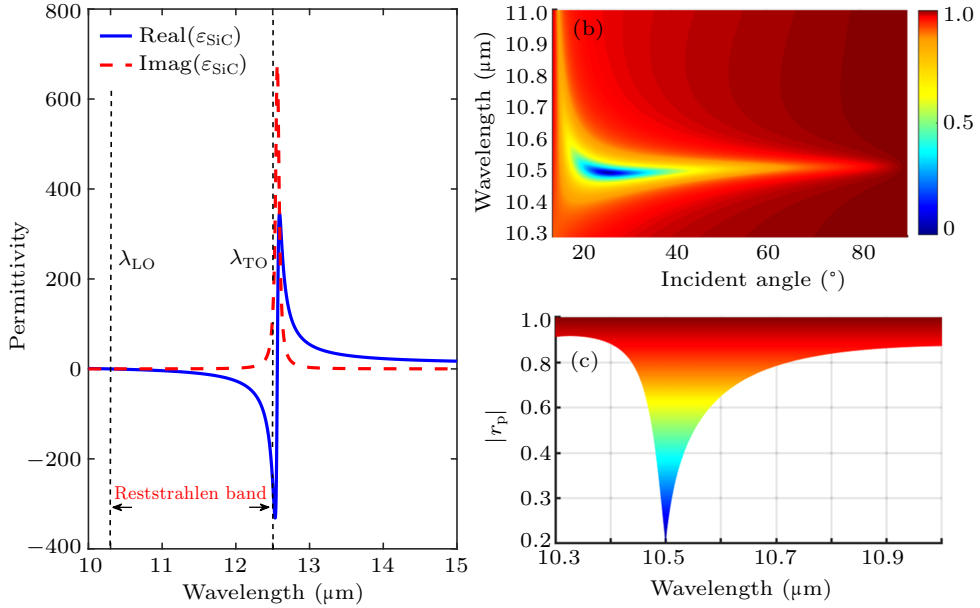



**Fig. 2.** (a) The complex permittivity of SiC and its reststrahlen band. (b) Variation of reflection coefficient $|r_p|$ with respect to the incident angle for the Ge prism–SiC–air structure under different incident wavelengths. (c) The reflection coefficient $|r_p|$ varies with the wavelength of incident light.

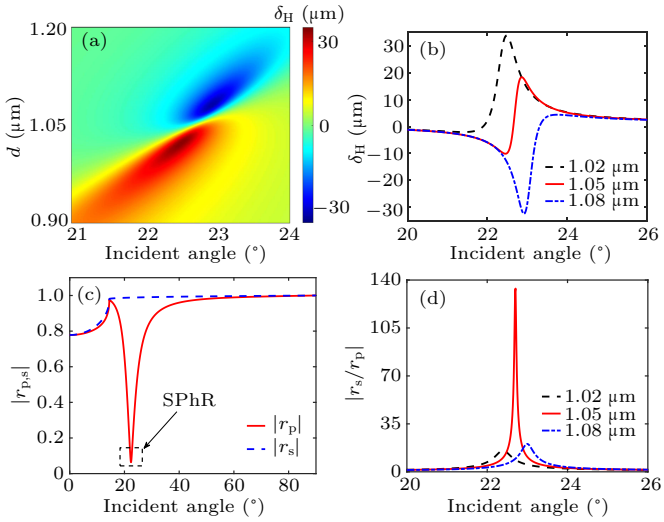



**Fig. 3.** (a) Dependences of transverse displacements $\delta_H$ as functions of the SiC film thickness and the incident angle at the incident wavelength of 10.6 μm. [(b), (d)] The variations of transverse displacements and the ratio $|r_s/r_p|$ at three different thicknesses of SiC layer. (c) Fresnel reflection coefficients changing with the incident angle under the optimal condition.

Figure 3(a) displays the transverse displacements of photonic SHE for Ge prism–SiC–air structure under different incident angles and SiC thicknesses. It is clearly seen that, the transverse displacements are very sensitive to the thickness of SiC layer, and the sign of displacement changes from positive to negative by increasing the SiC thickness. There should be an optimal parameter of SiC thickness to generate the prominent photonic SHE. Here, the transverse displacement *versus* the incident angle is shown in Fig. 3(b) with three different SiC thicknesses of 1.02 μm, 1.05 μm, and 1.08 μm. For the case of $d = 1.02$ μm, the transverse displacement presents an obvious peak of 33.9 μm at the incident angle of 22.4°. When the SiC thickness increases to 1.05 μm, the valley of transverse displacement becomes more pronounced, accompanied by the gradually decreased peak. Then a negative displacement of 32.4 μm is obtained at 22.9° with $d = 1.08$ μm. Therefore, the value of 1.02 μm may be the optimal SiC thickness for Ge prism–SiC–air structure, which results in the maximal positive transverse displacement of 33.9 μm. The Fresnel reflection coefficients as a function of incident angle under this optimal parameter are depicted in Fig. 3(c). Thereinto, $|r_s|$ changes monotonically with increasing the incident angle, and it keeps almost stable ($\sim 1$) under a large incident angle. Unlike $|r_s|$, there is a narrow resonance dip ($\sim 0.06352$) at 22.4° in the $|r_p|$ reflection curve, corresponding to notable SPhR effect in SiC-based Kretschmann–Raether configuration. For the case of $d = 1.05$ μm and 1.08 μm, the minimum $|r_p|$ are 0.007381 and 0.04874, respectively. As previous reports indicated, this condition of big $|r_s|$ and tiny $|r_p|$ would lead to a large ratio of $|r_s/r_p|$ around the resonance angle, conducive to the achievement of giant photonic SHE. Thus we describe the dependence of $|r_s/r_p|$ ratio versus the incident angle in Fig. 3(d). Obviously, both the maximal positive and negative displacements are partly attributable to the large value of $|r_s/r_p|$ ratio. When $d = 1.02$ μm and 1.08 μm, $|r_s/r_p|$ ratio gets 15.5 and 20.3 at the resonance angles of 22.4° and 22.9°, respectively, which are in agreement with the maximal displacements by SPhR effect around resonance angles. Note that, $|r_s/r_p|$ ratio reaches a larger value of 133.8 for $d = 1.05$ μm, however, the transverse displacements are not greater than that of $d = 1.02$ μm and 1.08 μm.

According to Eq. (6), the photonic SHE is closely related to the value of $|r_s/r_p|$, nevertheless, other items (e.g., $\partial \ln r_p/\partial\theta_i$) should also be considered. To demonstrate this conjecture, the effects of numerator $\mathrm{Re}(1+r_s/r_p)\cot\theta_i$, denominator $|(1+r_s/r_p)\cot\theta_i|^2$ and $\left|\partial \ln r_p/\partial\theta_i\right|^2$ on transverse displacements for $d = 1.02$ μm, 1.05 μm, and 1.08 μm are shown in Fig. 4. It is clearly found that the denominators $|(1+r_s/r_p)\cot\theta_i|^2$ and $\left|\partial \ln r_p/\partial\theta_i\right|^2$ are much more 3-orders of magnitude larger than the numerator $\mathrm{Re}(1+r_s/r_p)\cot\theta_i$, which also plays an essential role in determining the value of transverse displacements. More precisely, the denominators for $d = 1.05$ μm are about 30 times greater than the conditions of $d = 1.02$ μm and 1.08 μm, detrimental to the generation of giant photonic SHE. Hence, the transverse displacement for this proposed SPhR structure has intimate correlation with the magnitude of $|r_s/r_p|$ ratio, but other items (e.g., $\partial \ln r_p/\partial\theta_i$) cannot be neglected.

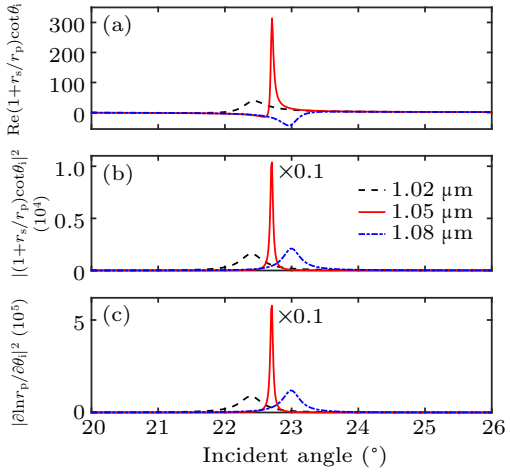



**Fig. 4.** The numerator $\mathrm{Re}(1+r_s/r_p)\cot\theta_i$, the denominator $|(1+r_s/r_p)\cot\theta_i|^2$, and the denominator $\left|\partial \ln r_p/\partial\theta_i\right|^2$ versus the incident angle in Eq. (6).

To further elucidate the underlying mechanism of this giant transverse displacements based on SPhR, we introduce the concepts of normal mode (spin maintenance without geometric phase) and abnormal mode (spin reflection with geometric phase).[36] Previous studies have demonstrated that when circularly polarized light is incident on the interface, both normal and abnormal modes are generated in the reflected beam. Similarly, for linearly polarized light incident on the interface, the internal spin components of the reflected beam can also be regarded as the combination of normal and abnormal

modes corresponding to different helicities. The reflection coefficient for the normal ($r_{\text{normal}}$) and the abnormal ($r_{\text{abnormal}}$) modes can be expressed as follows:[36] $r_{\text{normal}} = (r_{\text{p}} + r_{\text{s}})/2$, $r_{\text{abnormal}} = (r_{\text{p}} - r_{\text{s}})/2$. As illustrated in Fig. 5, the opposite sign (i.e., $r_{\text{normal}} = -r_{\text{abnormal}}$) appears at the resonance angle of 22.4°, thereby destructive interference between such modes leads to the vanishing of the reflection of the p-polarized incidence and then a significant photonic SHE.

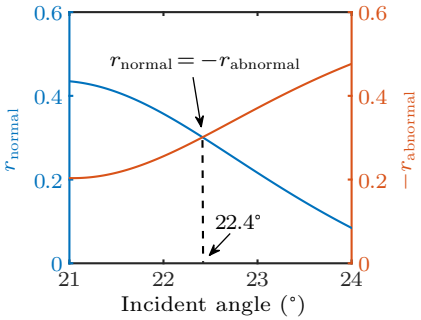



**Fig. 5.** Variation of Fresnel coefficients ($r_{\text{normal}}$, $r_{\text{abnormal}}$) with incident angle.

In addition to the incident wavelength of 10.6 μm, the transverse displacement of photonic SHE for Ge prism–SiC–air structure under different wavelengths of incident light has also been investigated, as exhibited in Table 1. To realize the strong photonic SHE, each wavelength corresponds to its optimal SiC thickness, and as the incident wavelength increases, the optimal thickness of SiC layer experiences a dramatic increase. For example, the optimal SiC thickness of 10.3 μm is only 30 nm (0.05 nm) to generate the maximal positive and negative transverse displacements, while it exceeds 1 μm for 10.6 μm. Moreover, the maximal transverse displacement firstly increases to a great value, and then it sharply declines with the increase of incident wavelength. For the case of 10.4 μm, the positive and negative transverse displacements simultaneously reach the giant values of 163.8 μm and −161.6 μm around the resonance angle of 23.6°, respectively. With the further increment of wavelength, both the positive and negative values of maximal transverse displacements are slightly decreased. As a consequence, by optimizing the incident wavelength to 10.4 μm, the calculated maximal transverse displacement of photonic SHE for this proposed SPhR structure (Ge prism–SiC–air) can be up to 163.8 μm, which is 55 times and 21 times that of photonic SHE enhanced by SPR and long-range SPR.[29,35] It is generally accepted that half of the incident beam waist ($w_0/2$) is the theoretical limit of transverse displacement.[16] The calculated value of 163.8 μm is about 0.65 times of the upper limit. The results suggest that, as a new mechanism, SPhR effect shows the promising potential to enhance the photonic SHE in the mid-infrared regime.

**Table 1.** The maximal positive and negative transverse displacements ($\delta_{+\max}$ and $\delta_{-\max}$) around resonance angles at different wavelengths of incident light, under the optimal SiC thickness.

| Wavelength (μm) | Resonance angle (°) | $d_+$ (nm) | $d_-$ (nm) | $\delta_{+\max}$ (μm) | $\delta_{-\max}$ (μm) |
|---|---|---|---|---|---|
| 10.3 | 14.6 | 30 | 0.05 | 15.4 | –28.1 |
| 10.4 | 23.6 | 330 | 332 | 163.8 | –161.6 |
| 10.5 | 26.5 | 649 | 654 | 125.5 | –126 |
| 10.6 | 22.4 | 1020 | 1080 | 33.9 | –32.4 |
| 10.7 | 19.5 | 1180 | 1430 | 15.5 | –12.2 |
| 10.8 | 18.4 | 950 | 1660 | 11.2 | –6.1 |

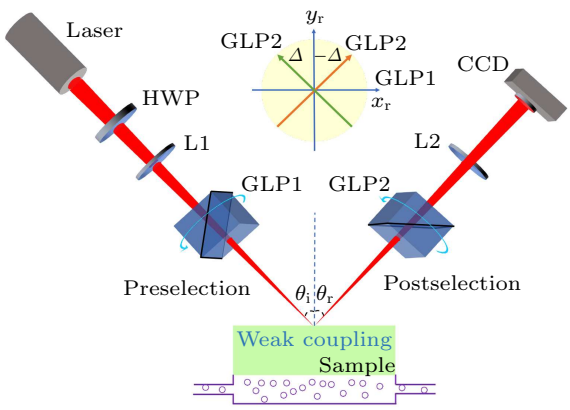



**Fig. 6.** The possible experimental setup: it is composed of laser, half-wave plate (modulating the intensity of the light field), two lenses (L1 for focusing the beam and L2 for collimating the reflected beam), two Glan laser polarizers (GLP1 and GLP2), CCD (a charge coupled device for detecting the signal, with the resolution of 1 μm),[32] and sensor structure (Ge prism–SiC–sensing). The illustration shows that the angle between the axes of GLP1 and GLP2 is $90° \pm \Delta$.

Given the close relationship between photonic SHE and refractive index changes of sensing medium, the photonic SHE opens up a novel platform for the refractive index detection of sensing medium. In comparison with other optical sensors, the photonic SHE sensors generally exhibit the superior sensitivity. Up to present, the refractive index sensors based on photonic SHE has been played an important role in the detection of harmful gases. Nitrogen dioxide ($NO_2$) is one of the major ambient air pollutants. Short-term (or long-term) exposure to high (or low) concentrations of $NO_2$ has caused catastrophic harm to human and animal health, and even death. Therefore, it is necessary to detect the concentration of $NO_2$ in the air. In this work, by taking advantage of the enhanced photonic SHE via SPhR, we develop a sensitive sensor based on the Ge prism–SiC–sensing structure (see in Fig. 1(a)) to detect $NO_2$ concentration. The possible experimental device is shown in Fig. 6, which is divided into three steps: preselection,

weak coupling, and postselection. For the refractive index of $NO_2$ and air mixture, we use the formula of linear interpolation: $n_{\text{mix}} = n_{NO_2} \cdot C_{NO_2} + n_{\text{air}} \cdot (1 - C_{NO_2})$,[37] where $C_{NO_2}$ is the concentration of $NO_2$ in the mixture, $n_{\text{air}} = 1.00027$, $n_{NO_2} = 1.40$.[38] The sensing performance of photonic SHE-based sensors can be evaluated by both intensity sensitivity and angle sensitivity. The intensity sensitivity is defined as $S_\delta = \Delta\delta/\Delta n_s$, where $\Delta\delta$ is the difference of transverse displacement (under a fixed incident angle) caused by a refractive index change $\Delta n_s$ of sensing medium. Similarly, $S_\theta = \Delta\theta/\Delta n_s$ is used to describe the angle sensitivity, in which $\Delta\theta$ is the variation of incident angle, corresponding to the peak/valley of transverse displacement.

For our proposed photonic SHE sensor, the transverse displacement is very sensitive to the refractive index variation of sensing medium. Since exposure to $NO_2$ at different concentrations has different levels of harm to the human body, we selected 0.5 ppm, 50 ppm, 100 ppm, 500 ppm, 1000 ppm, 1500 ppm, and 2000 ppm, and the corresponding refractive index range of the gas mixture is 1.00027–1.00107.[39] As depicted in Fig. 7(a), the transverse displacement undergoes a significant difference of 72.41 μm by fixing the incidence angle of 23.92°. Likewise, the incident angle corresponding to maximal negative transverse displacement varies from 24.1° to 23.92°, with the decreased $\Delta\theta$ of 0.18°. Figures 7(b) and 7(c) describe the transverse displacement and incident angle as a function of refractive index for sensing medium at different concentrations of $NO_2$, which basically exhibit the linear relation in the refractive index range of 1.00027–1.00107. Consequently, it is quite easy to obtain the sensitivity from the slope of the linear fitting curve. The calculated intensity and angle sensitivity of this $NO_2$ photonic SHE sensor are $9.07 \times 10^4$ μm/RIU and 237°/RIU, respectively.

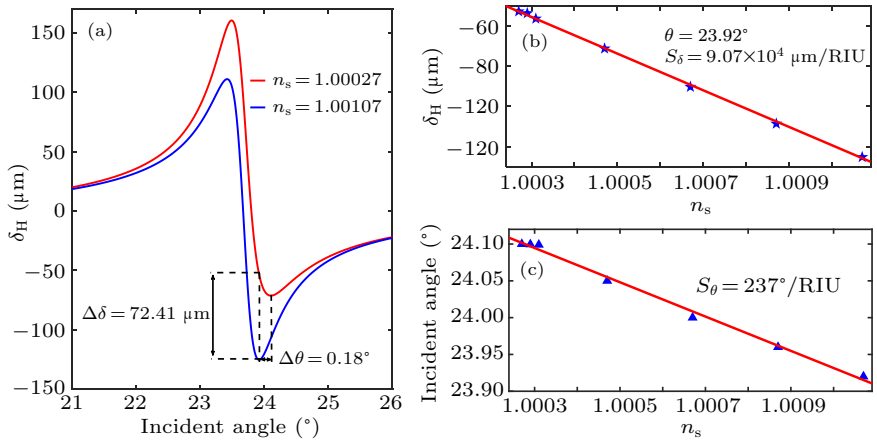



**Fig. 7.** (a) Description of intensity and angle sensitivity for photonic SHE-based sensor to detect $NO_2$ concentration. (b) and (c) Dependence of transverse displacement and incident angle on the refractive index of the sensing medium.

For our proposed SPhR structure, SiC is the fundamental material to excite surface phonon polaritons. In experiments, the growth of SiC on different substrates results in the alteration of damping rate $\gamma$, which will affect the refractive index of SiC,[3] as shown in Eq. (1). Therefore, the damping rate of SiC can be regarded as a new degree of freedom to manipulate the photonic SHE of SPhR structure and then the sensing performance. Figure 8(a) plots the relationship between the photonic SHE and damping rate of SiC. With the increase of damping rate, the resonance angle becomes gradually decreased; moreover, the tremendous differences take place in the positive and negative value of transverse displacements. When the damping rate is set to be $\gamma = 4$ cm$^{-1}$, the maximal transverse displacement of 152 μm is positive around the resonance angle of 22.8°. However, the transverse displacement for $\gamma = 6$ cm$^{-1}$ converts to a negative value of −120 μm at 19.8°. Therefore, the damping rate of SiC can be regarded as a new degree of freedom to manipulate the photonic SHE and then the sensing performance. Here, the sensitivity of $NO_2$ photonic SHE sensor versus damping rate is shown in Fig. 8(b) by further optimizing the thickness of SiC layer. It is clear that the sensing performance will sharply deteriorate when the damping rate of SiC exceeds a certain value ($\gamma > 4$ cm$^{-1}$). The sensing performance is excellent within the damping rate range of 3 cm$^{-1}$–4 cm$^{-1}$, the maximal intensity sensitivity and angle sensitivity can be up to $9.07\times10^4$ μm/RIU and 275°/RIU, respectively. Table 2 compares the sensitivity of our sensor with some other photonic SHE sensors based on SPR and SEP effects. From Table 2, the previously reported photonic SHE sensors based on SPR have the maximal intensity/angle sensitivity of $6.43\times10^5$ μm/RIU and 208°/RIU, respectively.[23,40] The maximum intensity/angle sensitivity of the SEP-based photonic SHE sensors is 6320.4 μm/RIU and 81°/RIU, respectively.[30,32] In this work, the calculated intensity sensitivity of our SPhR sensor is close to $10^5$ μm/RIU; meanwhile, the angle sensitivity reaches 275°/RIU. Therefore, the proposed photonic SHE sensor based on SPhR structure is extremely superior in both intensity and angle sensitivity, which demonstrates the excellent performance.

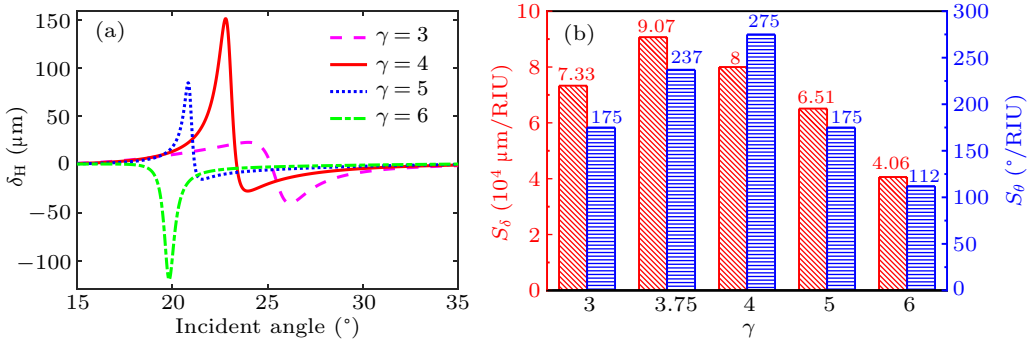



**Fig. 8.** (a) The relationship between transverse displacement and incident angle under different damping rates of SiC. (b) The influence of damping rate on intensity and angle sensitivity for SPhR-enhanced photonic SHE sensor to detect the $NO_2$ concentration.

**Table 2.** Comparison of our proposed sensor with some other photonic SHE sensors based on SPR and SEP effects.

| Structure | Intensity sensitivity (μm/RIU) | Angle sensitivity (°/RIU) | Mechanism | Reference |
|---|---|---|---|---|
| BK7–graphene–analyte–BK7 | $6.43\times10^5$ | 37.7 | SPR | [23] |
| Prism–gold–analyte–glass | – | 208 | SPR | [40] |
| Prism–TDBC–analyte | 6320.4 | – | SEP | [32] |
| Prism–Au–TDBC–analyte | – | 81 | SEP | [30] |
| Prism–SiC–analyte | $9.07\times10^4$ | 237 | SPhR | this work |

## 4. Conclusion

To summarize, the enhancement of photonic SHE and a highly sensitive refractive index sensor in the mid-infrared range are theoretical demonstrated by exploiting the strong excitation of SiC-supported SPhR. Under the optimal parameters of incident wavelength and SiC thickness, the calculated maximal transverse displacement of photonic SHE in Ge prism–SiC–air structure can reach as high as 163.8 μm, which is 55 times and 21 times that of photonic SHE enhanced by SPR and long-range SPR. Moreover, the damping rate of SiC can effectively control the photonic SHE and the sensing performance of our proposed SPhR-enhanced photonic SHE sensor for detecting $NO_2$ concentration in the air. The maximal intensity sensitivity and angle sensitivity are $9.07\times10^4$ μm/RIU and 275°/RIU, respectively, indicating the excellent sensing performance. These findings reveal the positive effect of SPhR on photonic SHE in SiC-based Kretschmann–Raether structure and offer the opportunity for developing highly sensitive photonic SHE sensors in the mid-infrared regime to detect harmful gases.

## Acknowledgements

Project supported by the National Natural Science Foundation of China (Grant No. 12175107), the Natural Science Foundation of Nanjing Vocational University of Industry Technology (Grant No. YK22-02-08), the Qing Lan Project of Jiangsu Province, the Natural Science Foundation of Jiangsu Province of China (Grant No. BK20230347), and the Fund from the Research Center of Industrial Perception and Intelligent Manufacturing Equipment Engineering of Jiangsu Province, China (Grant No. ZK21-05-09).

## References

[1] Shankaran D R, Gobi K V and Miura N 2007 *Sens. Actuators B* **121** 158
[2] Xu Y, Wu L and Ang L K 2019 *Phys. Rev. Appl.* **12** 024029
[3] Zheng G, Chen Y, Bu L, Xu L and Su W 2016 *Opt. Lett.* **41** 1582
[4] Valsecchi C and Brolo A G 2013 *Langmuir* **29** 5638
[5] Xu Y, Bai P, Zhou X, Akimov Y, Png C E, Ang L K, Knoll W and Wu L 2019 *Adv. Opt. Mater.* **7** 1801433
[6] Zhang J, Zhang L and Xu W 2012 *J. Phys. D: Appl. Phys.* **45** 113001
[7] Boltasseva A and Atwater H A 2011 *Science* **331** 290
[8] Wang T, Li P, Hauer B, Chigrin D N and Taubner T 2013 *Nano Lett.* **13** 5051
[9] Neuner III B, Korobkin D, Fietz C, Carole D, Ferro G and Shvets G 2009 *Opt. Lett.* **34** 2667
[10] Caldwell J D, Lindsay L, Giannini V, Vurgaftman I, Reinecke T L, Maier S A and Glembocki O J 2015 *Nanophotonics* **4** 44
[11] Caldwell J D, Glembocki O J, Francescato Y, Sharac N, Giannini V, Bezares F J, Long J P, Owrutsky J C, Vurgaftman I, Tischler J G, Wheeler V D, Bassim N D, Shirey L M, Kasica R and Maier S A 2013 *Nano Lett.* **13** 3690
[12] Zheng G, Xu L, Zou X and Liu Y 2017 *Appl. Surf. Sci.* **396** 711
[13] Zhang X, Wang Y, Zhao X, Huang T, Zeng S and Ping P S 2019 *IEEE Photonics J.* **11** 4800808
[14] Cao Y, Sheng L J, Cheng J H, Mei W and Ling X H 2024 *Opt. Laser Technol.* **174** 110583
[15] Liu Y, Ke Y, Luo H and Wen S 2017 *Nanophotonics* **6** 51
[16] Dong P, Wang G J and Cheng J 2021 *Chin. Phys. B* **30** 034202
[17] Bliokh K Y, Niv A, Kleiner V and Hasman E 2008 *Nat. Photonics* **2** 748
[18] Hosten O and Kwiat P 2008 *Science* **319** 787
[19] Ling X, Zhou X, Huang K, Liu Y, Qiu C W, Luo H and Wen S 2017 *Rep. Prog. Phys.* **80** 066401
[20] Zhou X, Xiao Z, Luo H and Wen S 2012 *Phys. Rev. A* **85** 043809
[21] Zhou X, Ling X, Luo H and Wen S 2012 *Appl. Phys. Lett.* **101** 251602
[22] Liu J, Zeng K, Xu W, Chen S, Luo H and Wen S 2019 *Appl. Phys. Lett.* **115** 251102
[23] Cheng J, Xiang Y, Xu J, Liu S and Dong P 2022 *IEEE Sens. J.* **22** 12754

[24] Sui J Y, Liao S Y, Li B and Zhang H F 2022 *Opt. Lett.* **47** 6065
[25] Wang R, Zhou J, Zeng K, Chen S, Ling X, Shu W, Luo H and Wen S 2020 *APL Photonics* **5** 016105
[26] Zhou X, Sheng L and Ling X 2018 *Sci. Rep.* **8** 1221
[27] Cheng J, Wang G, Dong P, Liu D, Chi F and Liu S 2022 *Chin. Phys. B* **31** 014205
[28] Li N, Tang T, Li J, Luo L, Li C, Shen J and Yao J 2019 *J. Magn. Magn. Mater.* **484** 445
[29] Zhou X and Ling X 2016 *IEEE Photonics J.* **8** 4801108
[30] Sahu S, Srivastava T and Jha R 2023 *Appl. Phys Lett.* **123** 203302
[31] Dong P, Xiang Y, Li R, Wang C, Cheng C and Cheng J 2023 *Ann. Phys.* **535** 2300309
[32] Yang W, Ang L K, Zhang W, Han J and Xu Y 2023 *Opt. Express* **31** 27041
[33] Barnes N P and Piltch M S 1979 *J. Opt. Soc. Am.* **69** 178
[34] Luo H, Zhou X, Shu W, Wen S and Fan D 2011 *Phys. Rev. A* **84** 043806
[35] Tan X J and Zhu X S 2016 *Opt. Lett.* **41** 2478
[36] Ling X, Xiao W, Chen S, Zhou X, Luo H and Zhou L 2021 *Phys. Rev. A* **103** 033515
[37] Passaro V M, Troia B and De Leonardis F 2012 *Sens. Actuators B* **168** 402
[38] Fulvio D, Sivaraman B, Baratta G A, Palumbo M E and Mason N J 2009 *Spectrochim. Acta, Part A* **72** 1007
[39] Mayorga M A 1994 *Toxicology* **89** 175
[40] Ahlawat L, Kamal K and Sinha R K 2024 *Opt. Laser Technol.* **170** 110183